Journal of Materials Chemistry A

RSC Publishing

PAPER

View Article Online
View Journal | View Issue



Cite this: J. Mater. Chem. A, 2013, 1, 954

# An integrated device for both photoelectric conversion and energy storage based on free-standing and aligned carbon nanotube film†

Zhibin Yang,‡[a] Li Li,‡[ab] Yongfeng Luo,[a] Ruixuan He,[a] Longbin Qiu,[a] Huijuan Lin[a] and Huisheng Peng*[a]

Received 29th August 2012
Accepted 30th October 2012

DOI: 10.1039/c2ta00113f

www.rsc.org/MaterialsA

An all-solid-state and integrated device in which photoelectric conversion and energy storage are simultaneously realized has been developed from free-standing and aligned carbon nanotube films or carbon nanotube–polyaniline composite films. Due to the aligned structure and excellent electronic property of the film electrode, the integrated device exhibits a high entire photoelectric conversion and storage efficiency of ~5.12%. The novel devices can also be flexible, and show promising applications in a wide variety of fields, particularly for portable electronic equipment.

## 1 Introduction

It is critically important to effectively store the electrical energy produced by solar cells.[1–3] Traditionally, they are connected to external energy storage devices such as various batteries through electrical wires. However, the relatively long distance connection has greatly decreased the storage efficiency. In addition, it is inconvenient for use and may not be allowed for many fields such as integratable and portable electronic devices. To further improve the use efficiency, a supercapacitor has been recently directly attached to an organic solar cell.[4–7] Specifically, the back electrode of the solar cell was contacted with an electrode of the supercapacitor. Although the photoelectric conversion and energy storage were thereby realized without a long connection of electric wires, they were two separate devices in nature. In particular, the interface between the two electrodes has largely limited the device efficiency and optimization. The attached two devices were also not flexible, although the possibility of being flexible has been considered as a main advantage in the development of high-performance devices.

On the other hand, due to their unique structure and excellent mechanical, electrical, and electrocatalytic properties, carbon nanotubes (CNTs) have been widely studied as electrodes in both photovoltaic and energy storage devices.[8–13] For dye-sensitized solar cells, CNT films have been used as both working and counter electrodes.[8,9] In the use of CNT film as a counter electrode, for instance, the resulting cells showed high power conversion efficiencies close to the conventional platinum. Supercapacitors based on CNT films as electrodes also exhibited a high performance, *e.g.*, a specific capacitance of 54 F $g^{-1}$.[14] Although CNTs have been widely used in either dye-sensitized solar cell or supercapacitor, no studies have been reported to integrate them into an effective device. In addition, the CNTs used typically appeared in a randomly dispersed structure, while aligned CNT materials were proposed to be more efficient.[11]

Herein, we have developed an all-solid-state and integrated device in which both photoelectric conversion and energy storage are realized on the basis of free-standing and aligned multi-walled carbon nanotube (MWCNT) films as electrodes. The structure of the integrated device is shown in Fig. 1 and S1.† Specifically, a gel or solid electrolyte was first sandwiched between two aligned MWCNT films to realize the energy

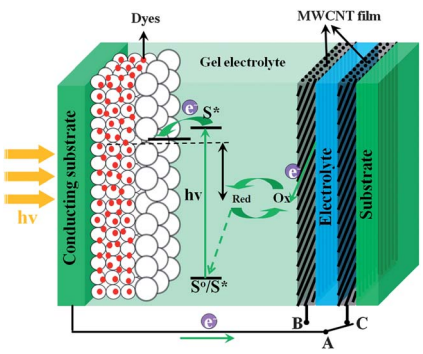


**Fig. 1** Schematic illustration of an integrated device for both photoelectric conversion and energy storage based on aligned MWCNT films as electrodes.

[a]State Key Laboratory of Molecular Engineering of Polymers, Department of Macromolecular Science, and Laboratory of Advanced Materials, Fudan University, Shanghai 200438, China. E-mail: penghs@fudan.edu.cn

[b]College of Food Science and Technology, Shanghai Ocean University, Shanghai 201306, China

† Electronic supplementary information (ESI) available. See DOI: 10.1039/c2ta00113f

‡ These authors contributed equally to this work.

storage. A dye-incorporated $TiO_2$ electrode was then integrated onto one of the MWCNT films to achieve the photoelectric conversion. Upon illumination by light, the photogenerated electrons from the dye molecules are injected into the conduction band of the $TiO_2$ nanoparticles, followed by them flowing to the MWCNT electrode by the external circuit. The aligned structure and high surface area of MWCNTs provide the integrated device with a high performance, *e.g.*, photoelectric conversion efficiency of 6.10%, specific capacitance of 48 F $g^{-1}$, and storage efficiency of ~84%. To improve the device performance, a second phase such as polyaniline (PANI) was further incorporated into the MWCNT film to increase the specific capacitance to 208 F $g^{-1}$. Due to the good flexibility of MWCNT films, ultrathin and flexible devices have also been produced with high performance. The novel device can be widely used in many fields, particularly for portable electronic equipment.

## 2 Experimental section

### 2.1 Preparation of aligned MWCNT films

MWCNT arrays were grown by a chemical vapor deposition with Fe (1 nm)/$Al_2O_3$ (10 nm) on silicon substrate as the catalyst typically at 750 °C (Fig. S2†).[15–19] Ethylene was used as carbon source, and a gas mixture of Ar and $H_2$ was used as carrier gas. The flow rates of Ar, $H_2$, and $C_2H_4$ were typically 400, 25, and 75 sccm, respectively. MWCNT arrays with a thickness of 2.0 mm were mainly used in this work. To prepare aligned MWCNT films, the MWCNT arrays grown on silicon substrate were fixed to a plate, followed by pressing with a glass slide (Fig. S3†). The resulting free-standing MWCNT film can be easily peeled off from the silicon substrate by a blade (Fig. S4†).

### 2.2 Preparation of MWCNT–PANI composite films

The composite film was synthesized by chemical oxidation polymerization of aniline monomers. Typically, ammonium persulfate (14.25 g) as the initiator was dissolved in deionized water (250 mL), and the monomer (4.65 mL) was dissolved in 1 M HCl solution (250 mL) under ultrasonic irradiation for 10 min. The as-prepared initiator and aniline solutions were then kept in an ice bath for 30 min. The cold initiator solution was dropped onto MWCNT films, followed by addition of the aniline solution after 20 s. The polymerization was performed at 4 °C for 2 min. Finally, the resulting composite films were washed with deionized water three times and dried under vacuum at 60 °C for 12 h.

### 2.3 Fabrication of integrated devices

The outer electrode in the photoelectric conversion part was composed of a layer of nanocrystalline $TiO_2$ particles (diameter of 20 nm) with thickness of 14 μm and a light-scattering layer of $TiO_2$ particles (diameter of 200 nm) with thickness of 2 μm on fluorine-doped tin oxide glass (15 ohm per square) prepared by a screen printing technology. The electrode was heated at 500 °C for 30 min and annealed in air. It was then immersed in 40 mM $TiCl_4$ aqueous solution at 70 °C for 30 min, followed by washing with de-ionized water and sintering at 500 °C for 30 min. For the flexible device, a $TiO_2$ mixture with 80% anatase and 20% rutile was added to ethanol at a concentration of 20 wt%, and the suspension was then coated onto the indium tin oxide on polyethylene naphthalate (15 ohm per square). The $TiO_2$ electrode at 120 °C was immersed into 0.3 mM *cis*-diisothiocyanato-bis(2,2′-bipyridyl-4,4′-dicarboxylato) ruthenium(II) bis-(tetrabutylammonium) (a dye also named N719) solution in a solvent mixture of dehydrated acetonitrile and *tert*-butanol (volume ratio of 1/1) for ~16 h. The N719-incorporated electrode was carefully rinsed with dehydrated acetonitrile. The gel electrolyte was coated onto the N719-incorporated electrode by a doctor blading method. The used area of the electrode was 0.36 $cm^2$. At the same time, a PVA–$H_3PO_4$ electrolyte was sandwiched between two aligned MWCNT films with a relatively large area of 1 $cm^2$ as the electrode. Here the PVA–$H_3PO_4$ electrolyte was prepared by dissolving PVA powder (1 g) in deionized water (10 mL) and $H_3PO_4$ (2 mL). The $TiO_2$ electrode was finally pressed onto one MWCNT film by use of a Surlyn frame (thickness of 60 μm) as the spacer at a pressure of ~0.2 MPa and introduction of a gel electrolyte as the photoactive component. The gel electrolyte for the photoelectric conversion part was prepared by mixing poly(vinylidene fluoride-*co*-hexafluoropropene) (10 wt%, Atochem, KynarFlex 2801) and 3-methoxypropionitrile solution containing 0.1 M LiI, 0.05 M $I_2$, 0.5 M 4-*tert*-butylpyridine and 0.5 M 1-propyl-2,3-dimethylimidazolium iodide.[20] The integrated device was finally obtained after sealing at 125 °C.

### 2.4 Characterization

The thickness of MWCNT films was measured by a Dektak 150 Step Profiler. The structure of MWCNT films was characterized by scanning electron microscopy (Hitachi FE-SEM S-4800 operated at 1 kV). The electrical conductivity was obtained by a physical property measurement system (KEITHLEY 2182A nanocoltmeter with 6221A DC and AC current source). The resistivity change under bending was monitored by an Agilent 34401A digital multimeter. Raman measurements were performed on a Renishaw inVia Reflex with an excitation wavelength of 514.5 nm and laser power of 2 mW at room temperature. The dye-sensitized solar cells were measured by recording *J–V* curves with a Keithley 2400 Source Meter under illumination (100 mW $cm^{-2}$) of simulated AM1.5 solar light coming from a solar simulator (Oriel-94023 equipped with a 450 W Xe lamp and an AM1.5 filter). The stray light was shielded by a mask with an aperture which was a little smaller than the working electrode. Cyclic voltammetry, galvanostatic charge/discharge and photocharging tests were performed on a CHI 660d electrochemical workstation.

## 3 Results and discussion

For the preparation of aligned bare MWCNT films, the thickness of MWCNT films was controlled by varying the height of MWCNT arrays. Typically, an array with a height of 1 mm produced a film with a thickness of 25 μm on a glass slide (Fig. S5†). MWCNT arrays with a height of 2 mm were mainly

used to produce MWCNT films with a thickness of ~50 μm in this work, unless otherwise specified. The angle between MWCNTs and the flat film was calculated to be ~1.4°. The resulting MWCNT film can be easily peeled off and coated onto various rigid and flexible substrates. These MWCNT films showed very high electrical conductivities close to individual MWCNTs ($10^4$ S cm$^{-1}$), compared with $10^0$ to $10^2$ S cm$^{-1}$ in the randomly dispersed or other aligned MWCNT films in the direction perpendicular to the film.[21–23] The high conductivity may greatly improve the charge transport in their use as electrodes. In addition, as the MWCNTs were highly aligned in the film (Fig. 2a), the in-plane conductivity achieved a high level of $10^2$ S cm$^{-1}$. The MWCNT films were highly flexible and stable. The conductivities of a MWCNT film varied by less than 2% in the above two cases after it was bent for one hundred cycles. The combined properties make them very promising as electrode materials in the devices for both photoelectric conversion and energy storage.[8,9,11,13]

To further improve the properties of MWCNT films, a second phase such as a polymer was often incorporated to produce composite films.[24,25] Here we have mainly introduced PANI with the advantages of easy synthesis and low cost.[24] Fig. 2b shows a scanning electron microscopy image of an aligned MWCNT–PANI composite film. PANI can be stably attached on MWCNTs due to their interactions. Raman spectra of PANI and MWCNT–PANI composites are shown in Fig. S6.† Compared with pure PANI, the stretching of C–N$^+$ shifted from 1338 to 1350 cm$^{-1}$ and the stretching of the benzene ring shifted from 1584 to 1594 cm$^{-1}$ in the MWCNT–PANI composite, which indicated the interaction between MWCNTs and PANI.[26,27]

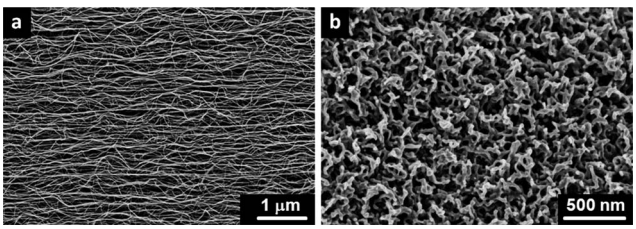


**Fig. 2** Scanning electron microscopy (SEM) images. (a) An aligned bare MWCNT film. (b) An aligned MWCNT–PANI composite film.

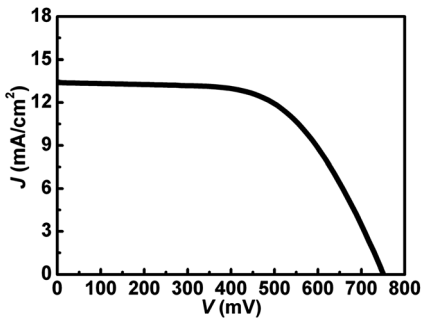


**Fig. 3** Photocurrent density–voltage (*J–V*) characteristics of an integrated device based on the aligned MWCNT film measured under AM1.5 illumination.

To investigate the photovoltaic performance of the integrated device, photocurrent density–voltage (*J–V*) characteristics were obtained under AM1.5 illumination (Fig. 3). It was found that, for both bare MWCNT and MWCNT–PANI composite films, the resulting integrated devices showed a similar photoelectric conversion efficiency ($\eta$) of 6.10% with open-circuit photovoltage ($V_{OC}$) of 0.750 V, short-circuit photocurrent density ($J_{SC}$) of 13.41 mA cm$^{-2}$ and fill factor (FF) of 0.61. The high photovoltaic performance is mainly derived from the high catalytic activity of MWCNTs due to high surface area.[28,29]

The energy storage part of integrated devices was characterized by cyclic voltammetry (CV) and galvanostatic charge/discharge tests. Fig. 4a and b show CV curves of integrated devices which were made from bare MWCNT and MWCNT–PANI composite films as electrodes and poly(vinyl alcohol)–$H_3PO_4$ (PVA–$H_3PO_4$) as electrolyte under different sweep rates of 10, 50, and 100 mV s$^{-1}$ at a potential range of 0 to 0.8 V. Supercapacitors are generally divided into two categories, *i.e.*, an electric double-layer capacitor in which the capacitance is derived from the charge separation at electrode–electrolyte interfaces and a pseudocapacitor with faradic reactions on the electrode.[30] The CV curve of the bare MWCNT film based device showed a rectangular shape without current peaks, indicating that the MWCNT film electrode possesses electrical double-layer capacitance (Fig. 4a).[31] In contrast, redox peaks were observed for the MWCNT–PANI composite film (25 wt% of PANI) based device (Fig. 4b), which indicated pseudocapacitance.[32] The current density based on the composite film was much higher than the bare MWCNT film. Accordingly, Fig. 4c and d further show the galvanostatic charge/discharge tests at a constant current density of 1.4 mA cm$^{-2}$. The discharge time of the MWCNT–PANI composite based device was ~140 s, much longer than the 35 s of the bare MWCNT film based device. The specific capacitances of bare MWCNT and MWCNT–PANI

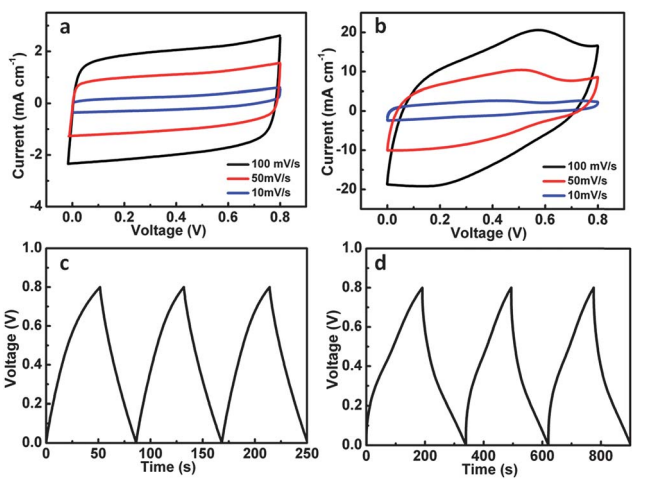


**Fig. 4** Electrochemical characterizations of bare MWCNT and MWCNT–PANI composite films as electrodes. (a and b) Cyclic voltammograms based on bare MWCNT and MWCNT–PANI composite films in PVA–$H_3PO_4$ electrolyte with different sweep rates of 10, 50, and 100 mV s$^{-1}$. (c and d) Galvanostatic charge/discharge curves based on bare MWCNT and MWCNT–PANI composite films, respectively. The thickness of the composite film was ~50 μm.

composite based devices were calculated to be 26 and 83 F $g^{-1}$, respectively. Inflection points were observed in the charge–discharge curve based on the MWCNT–PANI composite film, and they correspond to the redox potential where the redox reaction occurred during the charge–discharge process. The dependence of the specific capacitance on the electrode thickness for the two devices is further shown in Fig. S7.† The device based on the bare MWCNT film with thickness of 10 μm had a specific capacitance of 48 F $g^{-1}$. The capacitance continuously decreased with the increasing thickness of MWCNT films and stabilized at ~26 F $g^{-1}$. Compared with the bare MWCNT film, the device derived from an MWCNT–PANI composite film with the same thickness of 10 μm exhibited a much higher specific capacitance of 208 F $g^{-1}$. The specific capacitance also decreased with the increasing thickness of composite films. Here the same weight of PANI was used in all composite films. The device exhibited a high stability, *e.g.*, the voltage was maintained at 0.48 V after a self discharge of 400 s when it was charged to 0.8 V (Fig. S8†). In addition, the specific capacitance was slightly decreased by less than 5% after bending for 100 cycles (Fig. S9†).

Fig. 5a and b schematically show the photocharge and discharge of such an integrated device. Here the photocharge was performed under AM1.5 illumination, and the discharge was made by a galvanostatic method with a constant current density of 1.4 mA $cm^{-2}$. Fig. S10† shows the dynamic voltage of the integrated devices based on bare MWCNT and MWCNT–PANI composite films during the photocharging process. Obviously, the voltage was rapidly increased to and maintained at 0.72 V, which was slightly lower than $V_{OC}$ in the photoelectric conversion measurement, possibly due to the electric power lost in the external circuit. Fig. 5c and d further exhibit the curves of dynamic voltage *versus* time for the photocharge and galvanostatic discharge based on bare MWCNT and MWCNT–PANI composite films, respectively. The photocharge was much faster than the discharge due to a higher photocharging current density in both cases. For the bare MWCNT film based device, the voltage was increased to 0.72 V in ~8 s, while it took 35 s to complete the galvanostatic discharging process. The energy storage efficiency was calculated as ~84% with an entire photoelectric conversion and storage efficiency of ~5.12% (see ESI†). In the case of the MWCNT–PANI composite film, a longer photocharging time of 33 s was required, which indicated a better capability of charge loading. Accordingly, the galvanostatic discharge time was increased to ~144 s. The energy storage efficiency was calculated as ~70% with an entire photoelectric conversion and storage efficiency of ~4.29%. The lower energy storage efficiency for the MWCNT–PANI composite film can be mainly explained by the fact that, for the bare MWCNT film, the resulting device showed an electric double-layer capacitor behavior without chemical reactions during the charge/discharge processes, but for the composite film, some

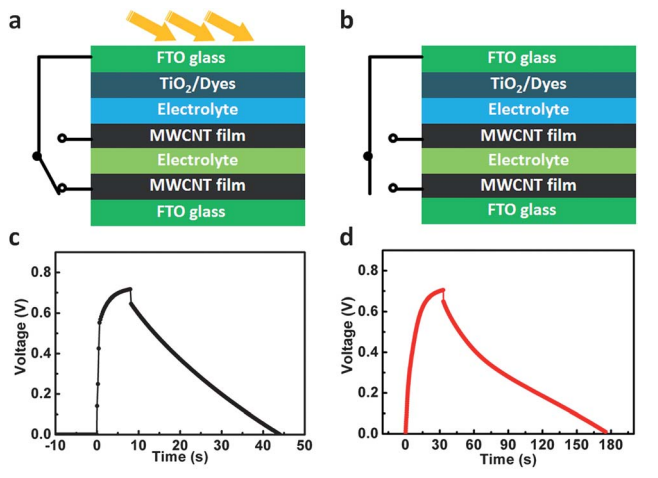


**Fig. 5** Schematic illustration and performance of an integrated device. (a and b) Schematic illustrations of an integrated device during photocharging and galvanostatic discharging processes, respectively. (c) The dynamic voltage of the device with bare MWCNT films as electrodes during photocharging and galvanostatic discharging processes. The constant discharge current density is 1.4 mA $cm^{-2}$. (d) The dynamic voltage of the device with MWCNT–PANI composite films as electrodes during photocharging and galvanostatic discharging processes. The characterizations were made in PVA–$H_3PO_4$ electrolyte under AM1.5 illumination. The constant discharge current density is 1.4 mA $cm^{-2}$.

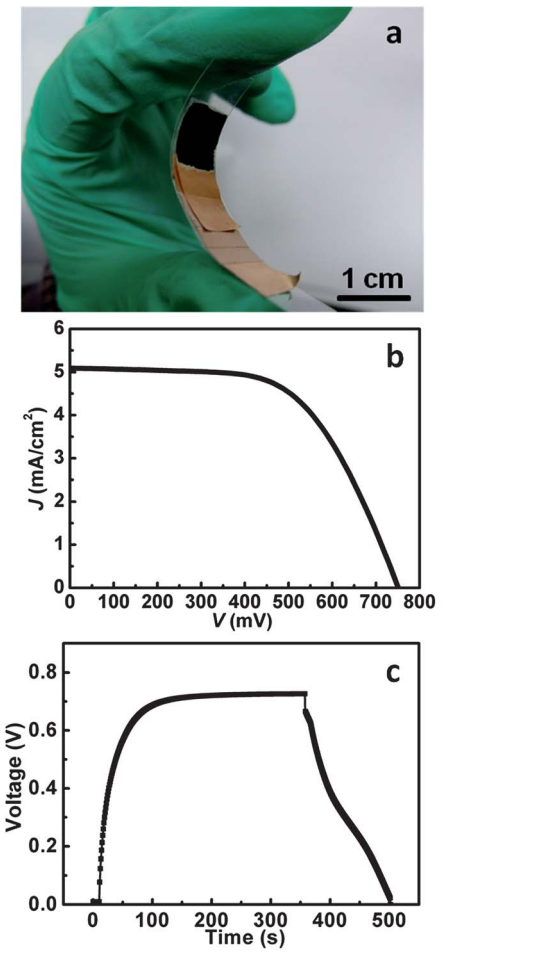


**Fig. 6** Photograph and characterization of a flexible integrated device. (a) Photograph of a flexible integrated device during bending. (b) Typical *J*–*V* curve under AM1.5 illumination. (c) The dynamic voltage during photocharging and galvanostatic discharging processes. The constant discharge current density is 1.4 mA $cm^{-2}$.

electrochemical reactions occurred for the consumption of charges. The cyclic stability of the integrated devices has also been investigated. The discharge capacitances remained almost unchanged for bare MWCNT films, and at least 80% was retained by the MWCNT–PANI composite film over 100 cycles.

As the aligned MWCNT films were highly flexible, a flexible integrated device was also easily fabricated (Fig. 6a). The resulting device on the basis of the MWCNT–PANI composite film showed a $V_{OC}$ of 0.75 V, $J_{SC}$ of 5.10 mA cm$^{-2}$, and FF of 0.61, which produced an $\eta$ of 2.31% (Fig. 6b). Fig. 6c further shows the voltage change during the photocharging and galvanostatic discharging processes. The flexible integrated device was photocharged to 0.73 V in 183 s and then maintained. Compared with the rigid counterpart, the relatively long photocharging time is mainly due to the lower photocurrent during the photocharge. The galvanostatic discharge time was about 137 s at a discharge current density of 1.4 mA cm$^{-2}$. The specific capacitance is 83 F g$^{-1}$, so the energy storage efficiency was calculated to be ~34% with an entire energy conversion and storage efficiency of 0.79%.

## 4 Conclusions

In summary, we have first developed an integrated device to realize both photoelectric conversion and energy storage by using aligned MWCNT films or composite films as electrodes. Due to the unique structure and remarkable property of the films, the resulting devices exhibited a high photoelectric conversion efficiency, high specific capacitance, and high storage efficiency. In addition, they could be flexible and easily integrated into portable electronic equipment. This work also provides an effective paradigm to fabricate various integrated devices by developing functional nanomaterials.

## Acknowledgements

This work was supported by NSFC (20904006, 91027025), MOST (2011CB932503, 2011DFA51330), MOE (NCET-09-0318), STCSM (11520701400, 12nm0503200), CPSF (2011M500724) and State Key Laboratory of Molecular Engineering of Polymers at Fudan University (K2011-10).

## Notes and references

1 W. Guo, X. Xue, S. Wang, C. Lin and Z. L. Wang, *Nano Lett.*, 2012, **12**, 2520–2523.
2 Q. Schiermeier, J. Tollefson, T. Scully, A. Witze and O. Morton, *Nature*, 2008, **454**, 816–823.
3 N. S. Lewis, *Science*, 2007, **315**, 798–801.
4 T. Miyasaka and T. N. Murakami, *Appl. Phys. Lett.*, 2004, **85**, 3932–3934.
5 T. N. Murakami, N. Kawashima and T. Miyasaka, *Chem. Commun.*, 2005, 3346–3348.
6 H. W. Chen, C. Y. Hsu, J. G. Chen, K. M. Lee, C. C. Wang, K. C. Huang and K. C. Ho, *J. Power Sources*, 2010, **195**, 6225–6231.
7 G. Wee, T. Salim, Y. M. Lam, S. G. Mhaisalkar and M. Srinivasan, *Energy Environ. Sci.*, 2011, **4**, 413–416.
8 T. Chen, S. Wang, Z. Yang, Q. Feng, X. Sun, L. Li, Z. S. Wang and H. Peng, *Angew. Chem., Int. Ed.*, 2011, **50**, 1815–1819.
9 G. Li, F. Wang, Q. Jiang, X. Gao and P. Shen, *Angew. Chem., Int. Ed.*, 2010, **49**, 3653–3656.
10 L. L. Zhang and X. Zhao, *Chem. Soc. Rev.*, 2009, **38**, 2520–2531.
11 H. Peng, *J. Am. Chem. Soc.*, 2008, **130**, 42–43.
12 L. Hu, J. W. Choi, Y. Yang, S. Jeong, F. La Mantia, L. F. Cui and Y. Cui, *Proc. Natl. Acad. Sci. U. S. A.*, 2009, **106**, 21490–21494.
13 M. D. Lima, S. Fang, X. Lepró, C. Lewis, R. Ovalle-Robles, J. Carretero-González, E. Castillo-Martínez, M. E. Kozlov, J. Oh and N. Rawat, *Science*, 2011, **331**, 51–55.
14 C. Yu, C. Masarapu, J. Rong, B. Wei and H. Jiang, *Adv. Mater.*, 2009, **21**, 4793–4797.
15 H. Peng and X. Sun, *Chem. Commun.*, 2009, 1058–1060.
16 P. D. Bradford, X. Wang, H. Zhao, J. P. Maria, Q. Jia and Y. Zhu, *Compos. Sci. Technol.*, 2010, **70**, 1980–1985.
17 D. Wang, P. Song, C. Liu, W. Wu and S. Fan, *Nanotechnology*, 2008, **19**, 075609.
18 H. Peng, X. Sun, F. Cai, X. Chen, Y. Zhu, G. Liao, D. Chen, Q. Li and Y. Lu, *Nat. Nanotechnol.*, 2009, **4**, 738–741.
19 M. Zhang, S. Fang, A. A. Zakhidov, S. B. Lee, A. E. Aliev, C. D. Williams, K. R. Atkinson and R. H. Baughman, *Science*, 2005, **309**, 1215–1219.
20 Y. L. Lee, Y. J. Shen and Y. M. Yang, *Nanotechnology*, 2008, **19**, 455201.
21 C. Berger, Y. Yi, Z. Wang and W. De Heer, *Appl. Phys. A: Mater. Sci. Process.*, 2002, **74**, 363–365.
22 A. Bachtold, M. Henny, C. Terrier, C. Strunk, C. Schönenberger, J. P. Salvetat, J. M. Bonard and L. Forro, *Appl. Phys. Lett.*, 1998, **73**, 274.
23 Z. Wu, Z. Chen, X. Du, J. M. Logan, J. Sippel, M. Nikolou, K. Kamaras, J. R. Reynolds, D. B. Tanner and A. F. Hebard, *Science*, 2004, **305**, 1273–1276.
24 C. Meng, C. Liu, L. Chen, C. Hu and S. Fan, *Nano Lett.*, 2010, **10**, 4025–4031.
25 V. L. Pushparaj, M. M. Shaijumon, A. Kumar, S. Murugesan, L. Ci, R. Vajtai, R. J. Linhardt, O. Nalamasu and P. M. Ajayan, *Proc. Natl. Acad. Sci. U. S. A.*, 2007, **104**, 13574.
26 T. M. Wu, Y. W. Lin and C. S. Liao, *Carbon*, 2005, **43**, 734–740.
27 L. Li, Z.-Y. Qin, X. Liang, Q.-Q. Fan, Y.-Q. Lu, W.-H. Wu and M.-F. Zhu, *J. Phys. Chem. C*, 2009, **113**, 5502–5507.
28 L. Li, Z. Yang, H. Gao, H. Zhang, J. Ren, X. Sun, T. Chen, H. G. Kia and H. Peng, *Adv. Mater.*, 2011, **23**, 3730–3735.
29 R. H. Baughman, A. A. Zakhidov and W. A. De Heer, *Science*, 2002, **297**, 787–792.
30 M. Yang, B. Cheng, H. Song and X. Chen, *Electrochim. Acta*, 2010, **55**, 7021–7027.
31 K. H. An, W. S. Kim, Y. S. Park, J. M. Moon, D. J. Bae, S. C. Lim, Y. S. Lee and Y. H. Lee, *Adv. Funct. Mater.*, 2001, **11**, 387–392.
32 F. Huang and D. Chen, *Energy Environ. Sci.*, 2012, **5**, 5833–5841.

 